ARTICLE   OPEN

Check for updates

More frequent central Pacific El Niño and stronger eastern pacific El Niño in a warmer climate

Na-Yeon Shin [1], Jong-Seong Kug [1,2 ✉], Malte F. Stuecker [3], Fei-Fei Jin [4], Axel Timmermann [5,6] and Geon-Il Kim [1]

El Niño events exhibit rich diversity in their spatial patterns, which can lead to distinct global impacts. Therefore, how El Niño pattern diversity will change in a warmer climate is one of the most critical issues for future climate projections. Based on the sixth Coupled Model Intercomparison Project simulations, we report an inter-model consensus on future El Niño diversity changes. Central Pacific (CP) El Niño events are projected to occur more frequently compared to eastern Pacific (EP) El Niño events. Concurrently, EP El Niño events are projected to increase in amplitude, leading to higher chances of extreme EP El Niño occurrences. We suggest that enhanced upper-ocean stability due to greenhouse warming can lead to a stronger surface-layer response for increasing positive feedbacks, more favorable excitation of CP El Niño. Whereas, enhanced nonlinear atmospheric responses to EP sea surface temperatures can lead to a higher probability of extreme EP El Niño.

INTRODUCTION

The El Niño–Southern Oscillation (ENSO) is the strongest air-sea coupled mode, which prominently governs Earth's interannual variability by modulating the global atmospheric circulation[1]. Important unresolved questions include how ENSO characteristics including amplitude, frequency, pattern, and asymmetry might change in response to greenhouse warming. Many studies have examined the response of ENSO to greenhouse warming[2–8], and there has been much interest in model consensus as to whether ENSO variability might strengthen or weaken[3–5,8–12]. Recent studies showed that the majority of Coupled Model Intercomparison Project phase 6 (CMIP6) models show an increase in ENSO variability including both EP and CP El Niño events in response to greenhouse warming[13,14], but still not for all models.

In contrast to these uncertain ENSO sea surface temperature (SST) variance changes, climate models are also projecting some more robust changes in ENSO characteristics. For example, the precipitation response to ENSO SST will likely be amplified[15] and shifted to the east[15,16]. The nonlinear atmospheric response to ENSO SSTs has been linked to projected more frequent extreme convective El Niño events[17,18], which often accompanies swings to extreme La Niña events in the following year[19].

ENSO has a rich diversity in terms of its spatial and temporal patterns[20–23]. Importantly, SST pattern diversity leads to distinct patterns of anomalous convection and in turn to different global impacts[24,25]. Therefore, it is critical to better understand how ENSO diversity might change under greenhouse warming. On one hand, it was suggested in an earlier study that the frequency of the central Pacific (CP) El Niño might increase in a warmer climate[26]. On the other hand, recent studies showed that eastern Pacific (EP) El Niño variability might increase in a warmer climate[13,27–29]. Though the two papers dealt with different aspects such as occurrence frequency and variability, the two aspects have been used interchangeably so a comprehensive understanding is still needed.

RESULTS

In this study, we revisit the projected changes in El Niño diversity under greenhouse warming using the latest generation of climate models that participated in CMIP6 (Supplementary Table 1). It has been reported that these CMIP6 models show improvements in the simulated ENSO and Pacific mean state[30]. These improvements may provide an opportunity to find new robust changes in projected future ENSO characteristics.

To examine El Niño's spatial diversity, we developed an algorithm to detect a longitude of the peak SST anomalies (SSTA)[31] (Methods). We first applied it to two observational SST datasets (Methods)[32,33]. The zonal distributions of the SSTA peak occurrences are shown in Fig. 1a,b. Both observational datasets exhibit a bimodal structure with maximums in the eastern and CP and an absence of peaks near 135°W, suggesting a clear separation into two groups of distinct events. We use this separation to classify CP and EP El Niño events, respectively. Even though several definitions of EP/CP events have been suggested[20–22,34,35], the present method may provide a more direct and intuitive view to describe ENSO pattern diversity. Composites of the two groups show distinct SSTA patterns, centered in the central, and eastern Pacific, respectively (Supplementary Fig. 1).

More frequent CP El Niño and Stronger EP El Niño in a warmer climate

Now, we apply this method to the CMIP6 simulations to determine the occurrences of each El Niño type. Figure 1c shows the zonal distribution of the El Niño SSTA peaks for the 20th century (1900–1999). Next, we calculate the multi-model ensemble (MME) average. Even though the central peak longitude histogram is

[1]Division of Environmental Science and Engineering, Pohang University of Science and Technology (POSTECH), Pohang, South Korea. [2]Institute for Convergence Research and Education in Advanced Technology, Yonsei University, Seoul, South Korea. [3]Department of Oceanography and International Pacific Research Center, School of Ocean and Earth Science and Technology (SOEST), University of Hawaiʻi at Mānoa, Honolulu, HI, USA. [4]Department of Atmospheric Sciences, School of Ocean and Earth Science and Technology (SOEST), University of Hawaiʻi at Mānoa, Honolulu, HI, USA. [5]Center for Climate Physics, Institute for Basic Science (IBS), Busan, South Korea. [6]Pusan National University, Busan, South Korea. ✉email: jskug@postech.ac.kr
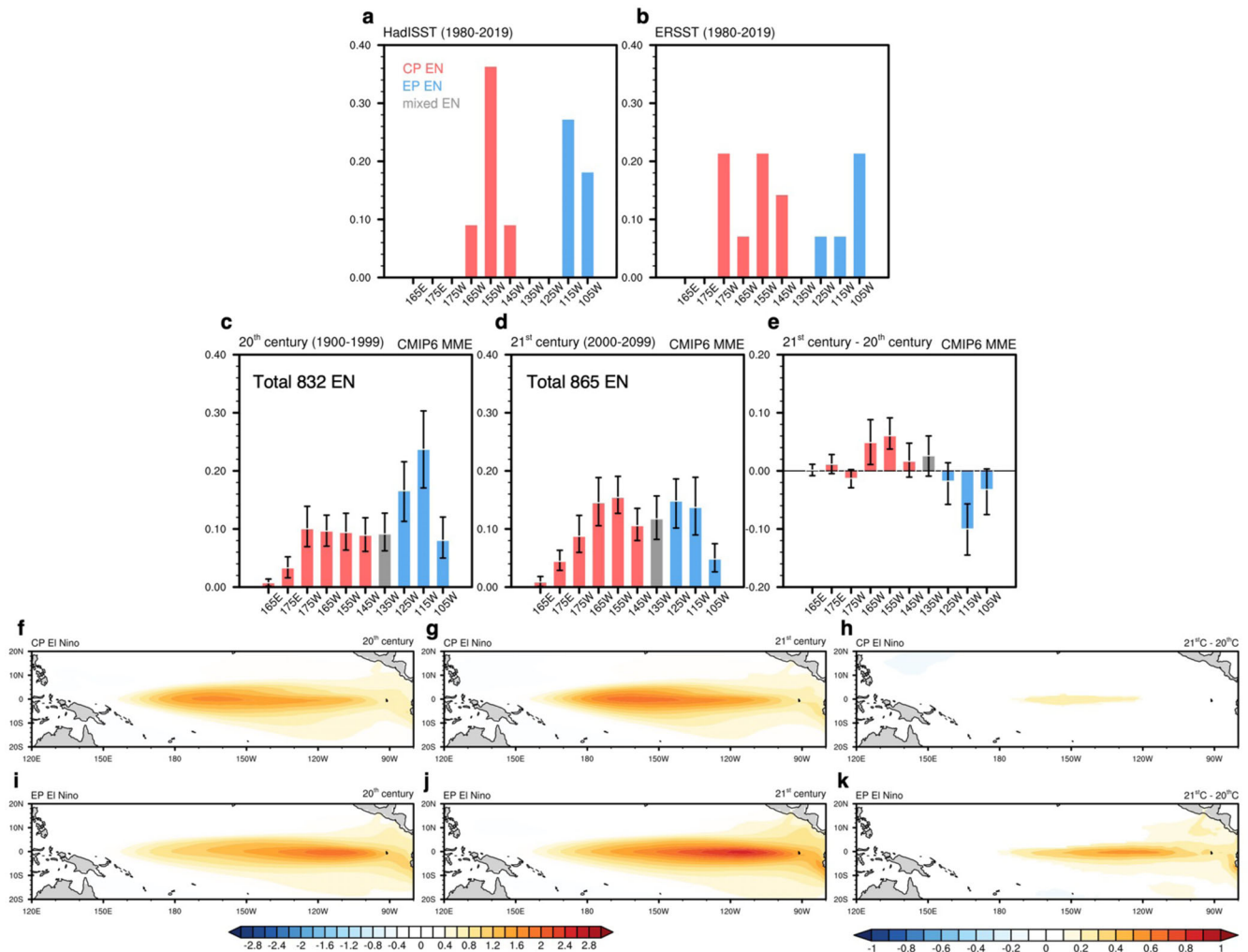
Fig. 1 Longitudinal distribution of El Niño SSTA center and its projected changes in the 21st century. a–e Histograms (normalized occurrences) of El Niño SSTA centers during November–December–January (NDJ) for ERSST (**a**), HadISST (**b**), as well as the MME of 30 CMIP6 models during the 20th century (1900–1999) (**c**), 21st century (2000–2099) (**d**), and their difference (**e**). Red, blue, and gray bars denote CP El Niño, EP El Niño, and mixed-type El Niño events, respectively. Error bars indicate the 95% confidence level obtained using the bootstrap method (Methods). **f–k** SSTA spatial patterns of each El Niño type in the CMIP6 MME: CP El Niño in the 20th century (**f**), 21st century (**g**), and difference (**h**). EP El Niño in the 20th century (**i**), 21st century (**j**), and difference (**k**). Values shown in shading are statistically significant at the 95% confidence level using the bootstrap method. The units are [**°C**] for (**f–k**).

smoothed out (i.e., less bimodal), possibly due to the MME, the CMIP6 MME shows a broad central Pacific peak (145–175°W) and sharp eastern peak (115–125°W) in the distribution. Based on this, we define CP and EP El Niño events following the same criteria as done for the observations. That is, El Niño events having their peak SSTA located between 165°E–145°W are defined as CP events and between 105–125°W as EP events. Small adjustments to the longitude criteria do not change the main conclusions of this study.

The models can simulate distinct SSTA patterns between the CP and EP El Niño events (Fig. 1f, h). In the 21st century (2000–2099), the models tend to simulate a more distinctive bimodal structure (Fig. 1d). The maximum probability of the CP peak is comparable to that of the EP peak. The difference in the histograms between the 21st and 20th centuries shows that the probabilities at 155–165°W are projected to significantly increase whereas the probability at 115°W is projected to significantly decrease (Fig. 1e). This suggests that CP El Niño events will occur more frequently in a warmer climate.

The spatial patterns of EP and CP El Niño events also show distinct features in the 21st century (Fig. 1g, i). It is interesting that the maximum location of SSTA during EP El Niño in the 21st century is slightly shifted to the west, compared to that in the present climate. This is consistent with the higher occurrence probability at 125°W compared to at 115°W (Fig. 1d). This suggests that SSTA peaks are westward shifted in the 21st century. In addition, the distribution for peaks of La Niña events also shows quite similar changes to that of El Niño events, indicating more frequent CP La Niña events in the CMIP6 models in the 21st century (Supplementary Fig. 2).

Even though the MME results show statistically significant changes in the occurrence of EP and CP El Niño events, we next investigate the changes in the individual models to obtain robust conclusions. Figure 2a shows how individual models simulate the occurrence frequencies of CP and EP El Niño events. To compare the occurrence frequency, the ratio of the CP events relative to the total number of both events (CP and EP El Niño) is calculated. Note that the results are consistent even if the ratio is calculated from the total number of all El Niño events: CP, EP, and mixed-type El Niño. For the MME, the ratio of CP El Niño significantly increases from 0.47 to 0.62 ($P < 0.05$). Among the 30 CMIP6 climate models, 25 models (83%) show an increased occurrence frequency of CP El
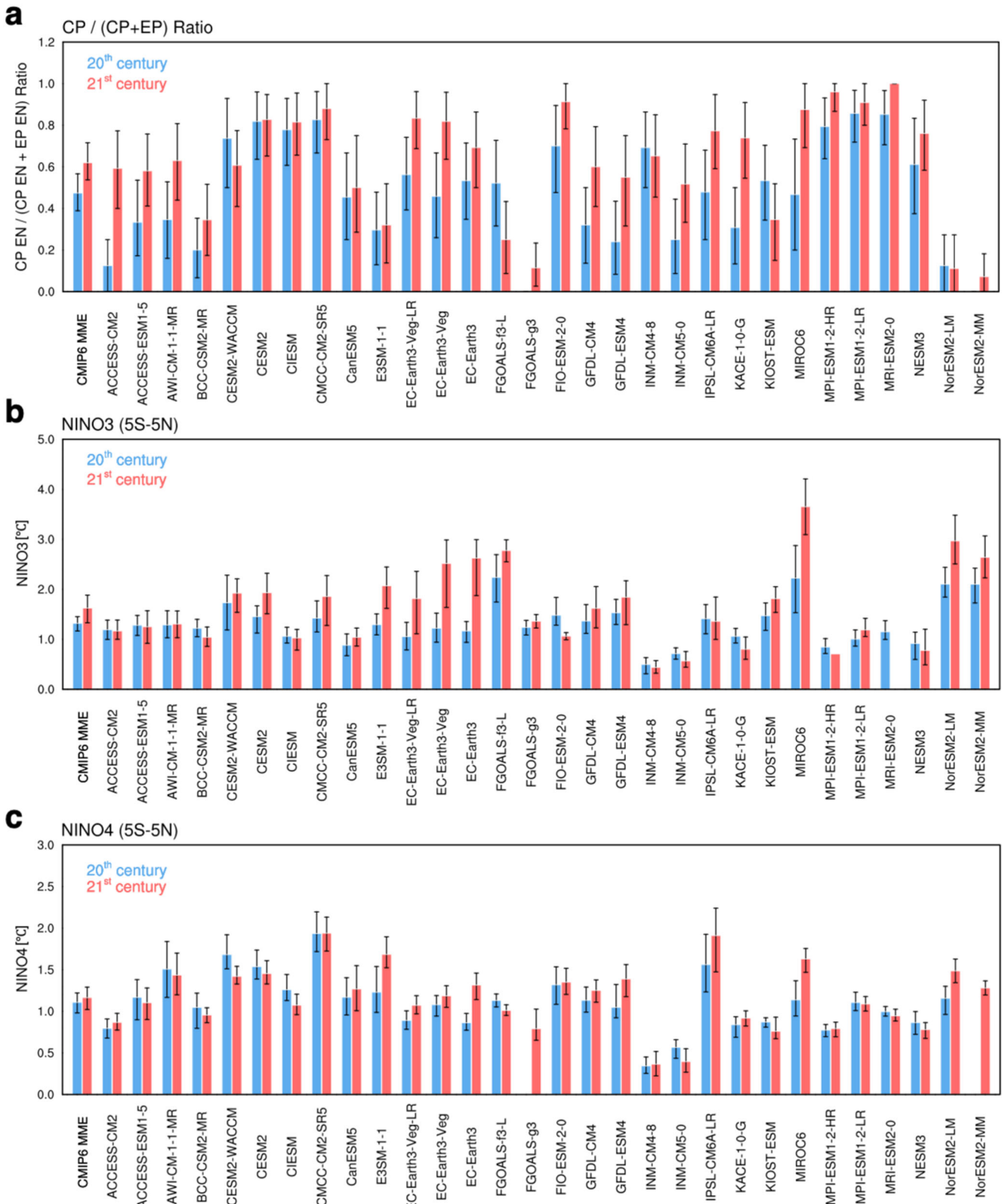
Fig. 2 Changes in frequency and magnitude in each type of El Niño. a Ratios of frequencies of CP El Niño events relative to the sum of the total number of CP and EP El Niño events. **b** The composites of Niño3 SSTA for EP El Niño events, and **c** Niño4 SSTA for CP El Niño events. Red and blue bars represent the 20th and 21st centuries, respectively. The error bars indicate the 95% confidence level using the bootstrap method (Methods). The units are [°C] for **b, c.**

NINO3

a 20th century

Moderate
44.4% ± 2.7
(404 ± 35)

Strong
45.4% ± 3.0
(409 ± 29)

Extreme
10.1% ± 2.1
(87 ± 16)

b 21st century

Moderate
41.8% ± 4.2
(396 ± 41)

Strong
42.9% ± 3.5
(407 ± 34)

Extreme
15.2% ± 3.9
(147 ± 39)

c Difference

NINO4

d 20th century

Strong
47.9% ± 3.4
(480 ± 35)

Extreme
4.5% ± 1.8
(41 ± 15)

Moderate
47.6% ± 3.5
(489 ± 56)

e 21st century

Strong
49.0% ± 4.7
(563 ± 67)

Extreme
6.7% ± 2.9
(73 ± 33)

Moderate
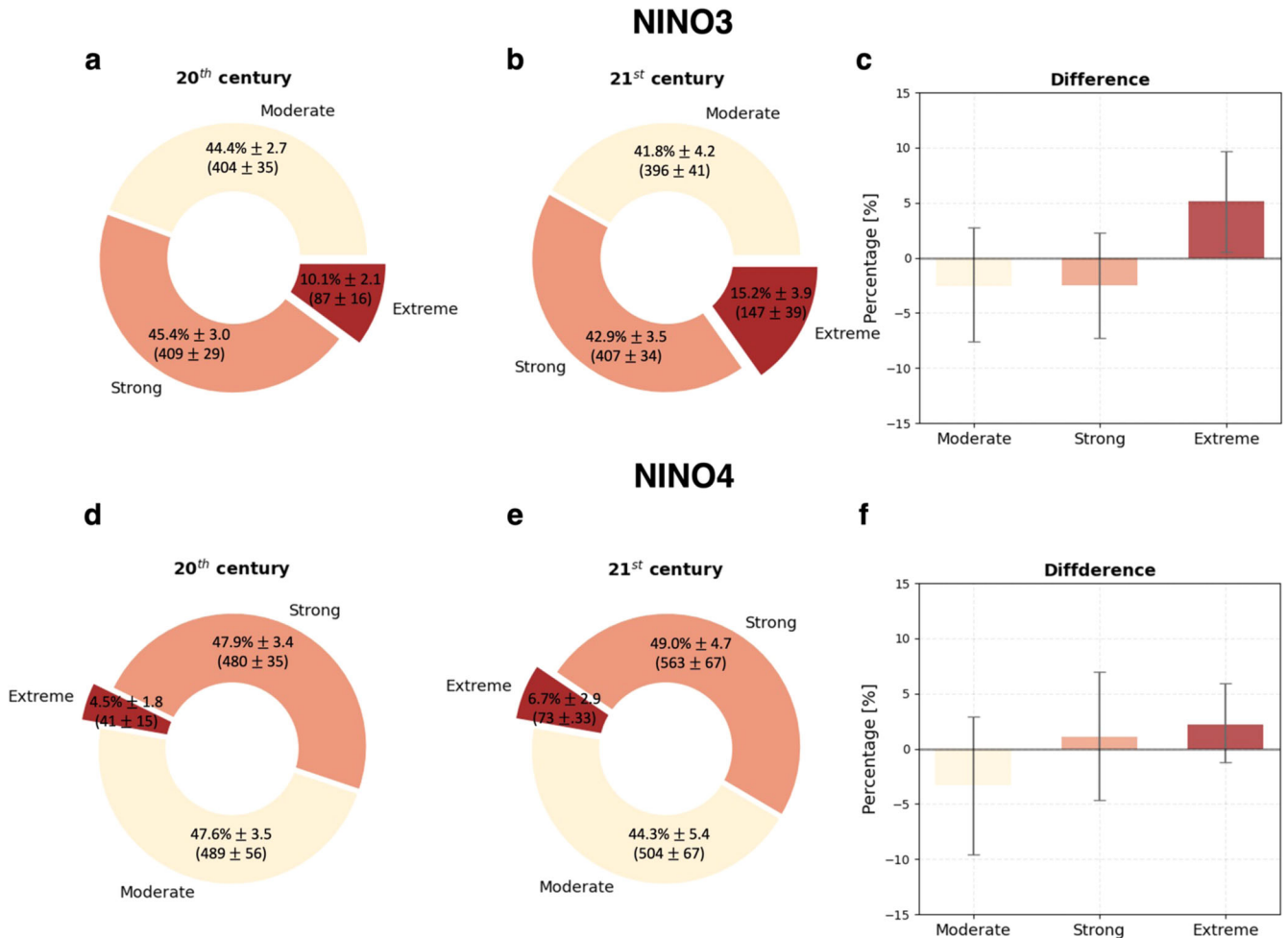44.3% ± 5.4
(504 ± 67)

f Diffderence

Fig. 3 Changes in extreme El Niño event occurrences in a warming climate. Ratios of moderate, strong, and extreme El Niño events in 30 CMIP6 models based on Niño3 SSTA (**a–c**) and Niño4 SSTA (**d–f**). **a**, **d** are for the 20th century, **b**, **e** 21st century, and **c**, **f** their difference, respectively. Each Niño index is normalized by STD of each model in the 20th century. Definitions of moderate, strong, and extreme El Niño events are based on [0.5–1STD], [1–2STD], and [>2STD], respectively. The value in parentheses is the number of events. The error bars indicate the 95% confidence level using the bootstrap method (Methods).

Niño events and only 5 models (17%) show a decrease. Even though the CMIP6 simulations show relatively large error bars due to the use of only one realization, 16 models show a statistically significant increase in CP El Niño occurrence, whereas only 2 models show a statistically significant decrease at the 95% confidence level, suggesting that the increased occurrence frequency of CP events under greenhouse warming is quite robust.

One notable change seen in Fig. 1f-i is that the SSTA is greater in the 21st century for both EP and CP events. In particular, the EP El Niño SSTA becomes considerably stronger. The intensified EP El Niño in response to greenhouse warming in the CMIP6 simulations was already reported by previous studies[11,13]. To determine ENSO amplitude changes of the individual models, Fig. 2b, c shows Niño3 and Niño4 SSTA composite anomalies of the EP and CP El Niño events, respectively, to examine the amplitude changes. On one hand, the MME average of the EP El Niño events shows about 23% increase of Niño3 SSTA in the 21st century (Fig. 2b). Among 30 models, 18 models simulate stronger Niño3 SSTA and 11 models simulate weaker Niño3 SSTA in the 21st century compared to the 20th century. On the other hand, the Niño4 SSTA associated with CP El Niño is projected to increase slightly in the 21st century, but it is not statistically significant from the inter-model spread. For individual models, 16 models simulate a strengthened CP El Niño and 12 models simulate a weakened CP

El Niño. Therefore, we conclude that the enhanced El Niño amplitude in the 21st century across CMIP6 models is more evident for the EP El Niño[13,27].

So far, we showed that the occurrences of CP El Niño events are projected to increase more than the occurrences of EP El Niño events in a warmer climate, but the magnitude of the EP El Niño becomes larger. The intensified EP El Niño amplitude with the decreased occurrence frequency can be explained by more extreme EP El Niño events. Figure 3 shows the ratio of moderate, strong, and extreme El Niño events to the total number of EP and CP El Niño events, respectively. The moderate, strong, and extreme EP El Niño (CP El Niño) events are defined when Niño3 (Niño4) SSTA are greater than 0.5, 1, and 2 standard deviation, respectively. In the present climate, extreme El Niño events account for about 10% of all EP El Niño events. However, the ratio of extreme El Niño events considerably increases to ~15% in the 21st century, which is consistent with some previous studies[13,27]. Therefore, the EP El Niño magnitude averaged over all EP El Niño events is increased. In contrast, extreme CP El Niño events account for about 4.5% of the total CP El Niño events, which is a much smaller fraction, possibly due to the negative skewness of Niño4 SSTA. Though the ratio of extreme CP El Niño is projected to increase slightly in the 21st century, this change may not contribute much to the overall amplitude change of CP El Niño events. In addition, extreme CP La Niña events are projected to
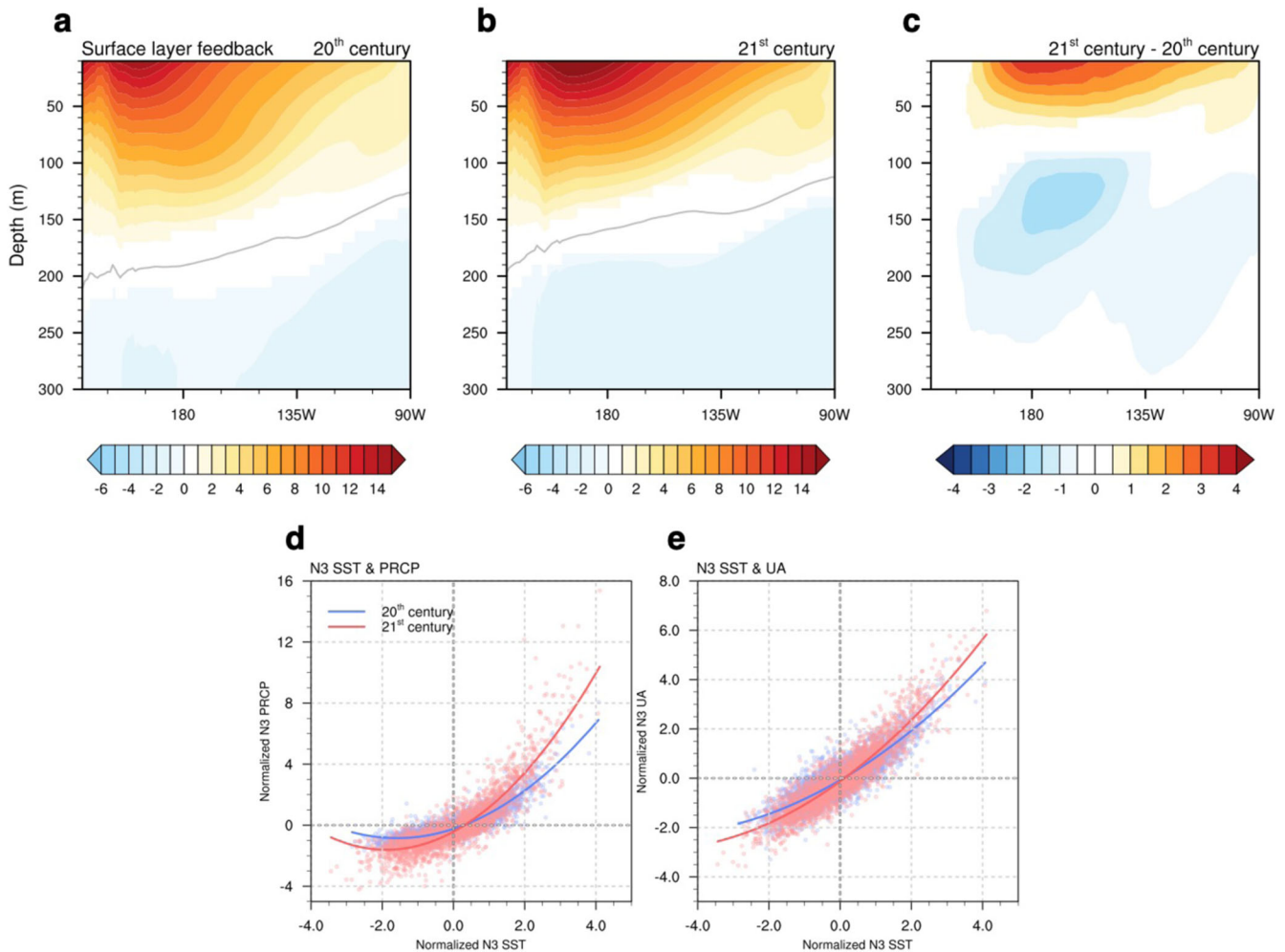
Fig. 4 Enhanced surface-layer feedback and increased nonlinear atmospheric feedback. The equatorial averaged (5°S–5°N) zonal current anomalies in response to the zonal-mean (5°S–5°N, 120°E–90°W) zonal windstress anomalies for the 20th century (**a**) and 21st century (**b**), respectively. Gray lines indicate the zero-line. Difference in zonal current response between the 20th and 21st centuries (**c**). Shadings indicate a 95% confidence level using the bootstrap method (Methods). The units are $[m^3\,N^{-1}\,s^{-1}]$ for (**a–c**). Scatter plots between precipitation anomalies and Niño3 SSTA (**d**) and between 850 hPa zonal wind anomalies and Niño3 SSTA (**e**) in the 30 CMIP6 models. Each variable is normalized by the 20th-century STD for each model. Blue and red colors represent the 20th and 21st centuries, respectively.

significantly increase (Supplementary Fig. 3), which is consistent with previous studies[13,19]. However, the increase of the extreme EP La Niña is not statistically significant.

Stronger surface-layer feedback and Nonlinear atmospheric feedback

It has been shown that projected future changes in El Niño diversity show more frequent CP El Niño and stronger EP El Niño events. Then, what causes these robust changes in the response to greenhouse warming? Previous studies suggested that enhanced upper-ocean stratification is responsible for projected changes in El Niño diversity[13,26,27]. Consistent with previous studies, the CMIP6 models commonly simulate enhanced stratification in the upper ocean (Supplementary Fig. 4). The faster warming in the surface layer[3,4] and the freshening due to the increased precipitation (Supplementary Fig. 5a)[36,37] together enhance the vertical density gradient, indicating stronger stratification. Furthermore, a weakened Walker circulation associated with an El Niño-like warming pattern (Supplementary Fig. 5b)[36] is related to a shoaling and deepening thermocline in the western Pacific and eastern Pacific, respectively, which leads to a colder subsurface in the western half of the Pacific basin (Supplementary Fig. 4a).

Therefore, the enhanced stratification is stronger in the western half of the Pacific, where wind anomalies associated with ENSO are the strongest.

The stronger stratification leads to stronger air-sea coupling[27]. That is, the surface layer responses to a given wind anomaly become stronger under the enhanced stratification[38–40], indicating stronger surface-layer feedback. To show the stronger surface-layer feedback, we calculated the zonal current response to the zonal-mean (120°E–90°W) zonal windstress anomaly forcing based on linear regression. In both simulations, the eastward current responses are stronger in the surface layer and become gradually weaker with the depth. There is also a westward current response below the thermocline, indicating a vertically baroclinic structure. However, the detailed structures are considerably different between the present and future simulations. While the eastward currents appear up to ~200 m over the western–CP in the 20th century (Fig. 4a), in the 21st century the eastward currents are confined up to ~160 m but the currents are much stronger in the surface layer (Fig. 4b). The difference between the 20th and 21st centuries clearly shows positive and negative in the surface and subsurface (below 100 m) layers (Fig. 4c), respectively, particularly in the western–CP, where a considerable shoaling of the mean thermocline takes place (Supplementary Fig. 4b). This difference

indicates that the current response to a given windstress forcing is concentrated in the surface layer in the warming simulation, suggesting a stronger surface-layer current response that directly affects SSTA development. The amplified surface-layer current response is particularly strong to the west of 135°W, where the SSTA center of CP El Niño is located.

The stronger surface-layer feedback plays an important role in controlling two major ENSO characteristics[41,42]. First, it leads to stronger ENSO variability by increasing positive feedbacks. In particular, it induces a stronger zonal advective feedback, which acts to shift the SSTA center westward[41]. Second, stronger surface-layer feedback can play a role in shortening the timescale of ENSO[42]. In particular, the enhanced zonal advective feedback plays a role in shifting the ENSO SSTA center westward, destabilizing the CP ENSO mode[42,43]. Therefore, more frequent CP El Niño occurrences could be explained by strengthened surface-layer feedback due to the enhanced ocean stratification.

The enhanced stratification can also strengthen the positive feedbacks associated with EP SSTA development, as well as CP SSTA development. For example, a strong stratification in the central Pacific can lead to a higher baroclinic mode of Kelvin waves[39] in the response to an anomalous westerly, which can lead to stronger thermocline and zonal current responses in the eastern Pacific. Even though the zonal current and thermocline responses are projected to increase in both CP and EP, the increase in zonal advective feedback and thermocline feedback[44] for the developing phase is the most dominant in CP and EP, respectively, in response to greenhouse warming (Supplementary Fig. 6 and Supplementary Table. 2). In particular, the increased zonal advective feedback in CP has strong inter-model consistency, and Ekman and thermocline feedbacks also slightly increased, while two feedbacks show different signs in EP. Therefore, in the warm climate, the CP SSTA might be more easily excited in the response to small perturbation of El Niño triggering factors such as the westerly wind bursts and equatorial ocean discharges[45], which lead to the more frequent occurrence of the CP El Niño.

Nevertheless, it is interesting that the EP El Niño event is projected to strengthen, and there will be a higher occurrence chance of extreme EP El Niño events. An enhanced nonlinear dynamical atmospheric response to ENSO SSTA in response to greenhouse warming may explain the higher probability of extreme EP El Niño events. It has been reported that the atmospheric response to the El Niño-related SSTA forcing tends to move eastward in models with an El Niño-like mean state warming pattern[3,15–17]. This eastward shift of the atmospheric response can be related to the extreme EP El Niño development[3,17,27].

Figure 4d shows the distribution of the eastern Pacific precipitation response depending on the magnitude of Niño3 SSTA across the CMIP6 models. The eastern Pacific precipitation anomaly exhibits a nonlinear response to Niño3 SSTA[18,46]. That is, the precipitation anomaly response is relatively weak for moderate Niño3 SSTA but increases nonlinearly as Niño3 SSTA increases. Since the eastern Pacific is a region of climatological atmospheric subsidence, small SSTA forcing cannot overcome the climatological sinking motion so the positive precipitation response is weak. Once sufficiently strong SSTA forcing induces a positive precipitation response against the sinking motion, it can further amplify through a positive precipitation-low level convergence feedback[47–49].

In response to greenhouse warming, an El Niño-like Pacific mean state warming pattern reduces the climatological sinking motion so that moderate SSTA forcing can be sufficient in inducing an eastern Pacific precipitation[15,18,36,50]. As shown in Fig. 4d, the 21st-century projections exhibit more events with strong positive SSTA and strong precipitation anomalies, consistent with more frequent extreme EP El Niño occurrences. In addition, we emphasize that the precipitation increase to a given SSTA increment is similar in the weak SSTA range in both centuries, but it becomes much steeper in the latter when Niño3 SSTA is greater than a certain threshold. The zonal wind anomalies also show a similar pattern to the precipitation anomalies (Fig. 4e). The threshold for the nonlinear positive atmospheric feedback is lower in the 21st century than in the 20th century, suggesting that the nonlinear atmospheric feedback intensifies. As a result, EP El Niño events can grow faster when the Niño3 SSTA passes the threshold. This might explain why in the 21st century we see a higher chance of extreme EP El Niño event occurrences, even though the total number of EP El Niño events decreases.

DISCUSSION
In this study, we showed that the latest generation of climate models shows a consensus on future changes in ENSO diversity. The most robust feature is that CP El Niño events are projected to occur more frequently in a warmer climate and that the occurrence of EP El Niño events will be less often. More frequent CP El Niño occurrences are consistent with results presented by Yeh et al.[26], but one may ask how they are linked to a study by Cai et al.[27], which pointed out the enhanced variance of EP El Niño SSTA in a warmer climate. Even though the total occurrence of EP El Niño is reduced in a warmer climate, their SSTA amplitude is increased in many models due to more frequent extreme EP El Niño. A higher probability of extreme EP El Niño occurrences is consistent with a study by Cai et al.[27]. An intensified nonlinear atmospheric dynamical response can lead to more extreme EP El Niño events.

In addition, the question of how one defines EP and CP El Niño events should be taken into account for the interpretation. When we use an EOF-based definition[35], we find that CP El Niño event occurrence does not increase in the 21st century compared to the 20th century (Supplementary Fig. 7). Instead, the centers of EP El Niño SSTA maxima are shifted to the west in the 21st century (Supplementary Fig. 8), which is consistent with our results to some extent (Fig. 1). Since an EOF-based definition[35] uses a fixed pattern and depends on where each model simulates the largest variability, the classification is sometimes different from a definition based on the actual location of the SSTA center. For example, if a model simulates dominant SSTA variability in the central Pacific due to the model bias, the model's EP El Niño pattern is shifted to the west. Therefore, the ratio of CP El Niño does not increase, but the center of EP El Niño can be shifted westward. As a result, it should be recognized that stronger EP El Niño variability based on an EOF definition[35] may represent stronger variability in the region where the model's SSTA variations are dominant. In this sense, our detection method might be more intuitive to describe changes in El Niño pattern diversity.

Regardless of the definitions, stronger surface-layer feedback due to the enhanced stratification plays a role in shifting the SSTA center to the west, which drives robust changes in El Niño diversity in response to greenhouse warming. In addition, it may suggest that the current 2–dimensional thinking on El Niño diversity may limit a more comprehensive understanding of ENSO in the presence of El Niño complexity[23,51].

METHODS
Observed data and model outputs
Detecting the longitudinal peak of ENSO sea surface temperature anomalies (SSTA) is conducted with two SST reanalysis datasets. The NOAA Extended Reconstructed Sea Surface Temperature version 5[32] at 2° × 2° horizontal resolution and the Hadley Center Sea Ice and Sea Surface Temperature version 1.1 at 1° × 1°

resolution[33] are used for the 1980 to 2019 time period. The method is also applied to 30 Coupled Model Intercomparison Project phase 6 (CMIP6) Coupled Global Climate Models (CGCMs; Supplementary Table 1). We use the historical (1900–2014) and Shared Socio-economic Pathway (SSP) 5–8.5 scenario experiments (2015–2100). We use the 1900–2099 period (200 years). Using monthly data, we removed the climatology and linearly detrended for each time period. Considering the seasonal variance modulation of ENSO, we focus the analysis on the November–December–January (NDJ) season.

Detecting center method

The algorithm to detect the longitudinal peak of ENSO SSTA is similar to Shin et al.[31]. The algorithm finds the local maximum SSTA along the equator. First, we average the detrended NDJ SSTA over 2°S–2°N. Second, we calculate a moving average with a 30° longitude window moved in 10° intervals (150°E–90°W; 10 points). Third, we select the points where the moving averaged NDJ SSTA is greater (less) than 1STD (-1STD). The STD is calculated for all months SSTA over 150°E–90°W. Among the selected points, the point having the largest absolute value is defined as a peak of El Niño (La Niña). The longitude where the peak is located is detected as the center of ENSO. For CMIP6 CGCMs, we calculate the STD for each model for each 100-year period.

Statistical significance test

To examine the statistical significance of projected changes, we use the bootstrap method in the following ways. (1) Inter-model consensus. We carry out random sampling of 30 models with replacement 10,000 times (Figs. 1c–i, 3, 4a–c). (2) Consistency in each type of El Niño or La Niña. We calculate the probability by randomly sampling as many as the number of each type of ENSO in each model with replacement 10,000 times (Fig. 2b, c). (3) Consensus of the occurrence change in CP El Niño in each model. Since we have 100 years for each period, we obtain the ratio from the dataset which is randomly sampled during these 100 years with replacement 10,000 times (Fig. 2a).

DATA AVAILABILITY

The CMIP6 archives are freely available from https://esgf-node.llnl.gov/projects/cmip6/. The ERSST version 5, monthly reanalysis data are available from https://www.esrl.noaa.gov/psd/data/gridded/data.noaa.ersst.v5.html. The HadISST version 1.1, monthly reanalysis data are available from https://www.metoffice.gov.uk/hadobs/hadisst/data/download.html.

CODE AVAILABILITY

The codes used to produce these results are available from the corresponding author upon reasonable request.

REFERENCES

1. McPhaden, M. J., Zebiak, S. E. & Glantz, M. H. ENSO as an integrating concept in earth science. *Science* **314**, 1740–1745 (2006).
2. Berner, J., Christensen, H. M. & Sardeshmukh, P. D. Does ENSO regularity increase in a warming climate? Does ENSO regularity increase in a warming climate? *J. Clim.* **33**, 1247–1259 (2019).
3. Cai, W. et al. ENSO and greenhouse warming. *Nat. Clim. Change* **5**, 849–859 (2015).
4. Collins, M. et al. The impact of global warming on the tropical Pacific Ocean and El Niño. *Nat. Geosci.* **3**, 391–397 (2010).
5. Stevenson, S. L. Significant changes to ENSO strength and impacts in the twenty-first century: results from CMIP5. *Geophys. Res. Lett.* **39**, L17703 (2012).
6. Taschetto, A. S. et al. Cold tongue and warm pool ENSO events in CMIP5: mean state and future projections. *J. Clim.* **27**, 2861–2885 (2014).
7. Yeh, S.-W., Ham, Y.-G. & Lee, J.-Y. Changes in the tropical pacific SST trend from CMIP3 to CMIP5 and its implication of ENSO*. *J. Clim.* **25**, 7764–7771 (2012).
8. Wengel, C. et al. Future high-resolution El Niño/Southern Oscillation dynamics. *Nat. Clim. Change* **11**, 758–765 (2021).
9. DiNezio, P. N. et al. Mean climate controls on the simulated response of ENSO to increasing greenhouse gases. *J. Clim.* **25**, 7399–7420 (2012).
10. Kim, S. T. et al. Response of El Niño sea surface temperature variability to greenhouse warming. *Nat. Clim. Change* **4**, 786–790 (2014).
11. Fredriksen, H., Berner, J., Subramanian, A. C. & Capotondi, A. How does El Niño–southern oscillation change under global warming—a first look at CMIP6. *Geophys. Res. Lett.* **47**, e2020GL090640 (2020).
12. IPCC. 2021: Climate Change 2021: The Physical Science Basis. Contribution of working group i to the sixth assessment report of the intergovernmental panel on climate change [Masson-Delmotte, V. et al. (eds.)]. *Cambridge University Press* (2021).
13. Cai, W. et al. Changing El Niño–Southern oscillation in a warming climate. *Nat. Rev. Earth Environ.* **2**, 628–644 (2021).
14. Cai, W. et al. Increased ENSO sea surface temperature variability under four IPCC emission scenarios. *Nat. Clim. Change* **12**, 228–231 (2022).
15. Power, S., Delage, F., Chung, C., Kociuba, G. & Keay, K. Robust twenty-first-century projections of El Niño and related precipitation variability. *Nature* **502**, 541–545 (2013).
16. Kug, J.-S., Ham, Y.-G., Lee, J.-Y. & Jin, F.-F. Improved simulation of two types of El Niño in CMIP5 models. *Environ. Res. Lett.* **7**, 034002 (2012).
17. Wang, G., Cai, W. & Santoso, A. Stronger increase in the frequency of extreme convective El Niño than extreme warm El Niño under greenhouse warming Stronger increase in the frequency of extreme convective El Niño than extreme warm El Niño under greenhouse warming. *J. Clim.* **33**, 675–690 (2019).
18. Cai, W. et al. Increasing frequency of extreme El Niño events due to greenhouse warming. *Nat. Clim. Change* **4**, 111–116 (2014).
19. Cai, W. et al. Increased frequency of extreme La Niña events under greenhouse warming. *Nat. Clim. Change* **5**, 132–137 (2015).
20. Ashok, K., Behera, S. K., Rao, S. A., Weng, H. & Yamagata, T. El Niño Modoki and its possible teleconnection. *J. Geophys. Res.* **112** (2007).
21. Kao, H.-Y. & Yu, J.-Y. Contrasting eastern-Pacific and central-pacific types of ENSO. *J. Clim.* **22**, 615–632 (2009).
22. Kug, J.-S., Jin, F.-F. & An, S.-I. Two types of El Niño events: cold tongue El Niño and warm pool El Niño. *J. Clim.* **22**, 1499–1515 (2009).
23. Timmermann, A. et al. El Niño–southern oscillation complexity. *Nature* **559**, 535–545 (2018).
24. Capotondi, A. et al. Understanding ENSO diversity. *Bull. Am. Meteorol. Soc.* **96**, 921–938 (2015).
25. Kim, S. & Kug, J. What controls ENSO teleconnection to East Asia? Role of Western North Pacific precipitation in ENSO teleconnection to east asia. *J. Geophys. Res. Atmos.* **123**, 10,406–10,422 (2018).
26. Yeh, S.-W. et al. El Niño in a changing climate. *Nature* **461**, 511–514 (2009).
27. Cai, W. et al. Increased variability of eastern Pacific El Niño under greenhouse warming. *Nature* **564**, 201–206 (2018).
28. Carréric, A. et al. Change in strong eastern Pacific El Niño events dynamics in the warming climate. *Clim. Dynam.* **54**, 901–918 (2020).
29. Lopez, H., Lee, S.-K., Kim, D., Wittenberg, A. T. & Yeh, S.-W. Projections of faster onset and slower decay of El Niño in the 21st century. *Nat. Commun.* **13**, 1915 (2022).
30. Planton, Y. Y. et al. Evaluating climate models with the CLIVAR 2020 ENSO metrics package. *Bull. Am. Meteorol. Soc.* **102**, 1–57 (2020).
31. Shin, N.-Y., Kug, J.-S., McCormack, F. S. & Holbrook, N. J. The double-peaked El Niño and its physical processes. *J. Clim.* **34**, 1291–1303 (2021).
32. Huang, B. et al. Extended reconstructed sea surface temperature, version 5 (ERSSTv5): upgrades, validations, and intercomparisons. *J. Clim.* **30**, 8179–8205 (2017).
33. Rayner, N. A. et al. Improved analyses of changes and uncertainties in sea surface temperature measured in situ since the mid-nineteenth century: the HadSST2 dataset. *J. Clim.* **19**, 446–469 (2006).
34. Ren, H. & Jin, F. Niño indices for two types of ENSO. *Geophys. Res. Lett.* **38** (2011).
35. Takahashi, K., Montecinos, A., Goubanova, K. & Dewitte, B. ENSO regimes: reinterpreting the canonical and Modoki El Niño. *Geophys. Res. Lett.* **38** (2011).
36. Xie, S.-P. et al. Global warming pattern formation: sea surface temperature and rainfall*. *J. Clim.* **23**, 966–986 (2010).
37. Huang, P., Xie, S.-P., Hu, K., Huang, G. & Huang, R. Patterns of the seasonal response of tropical rainfall to global warming. *Nat. Geosci.* **6**, 357–361 (2013).
38. Dewitte, B., Yeh, S.-W., Moon, B.-K., Cibot, C. & Terray, L. Rectification of ENSO variability by interdecadal changes in the equatorial background mean state in a CGCM simulation. *J. Clim.* **20**, 2002–2021 (2007).

39. Dewitte, B., Reverdin, G. & Maes, C. Vertical structure of an OGCM simulation of the equatorial Pacific Ocean in 1985–94. *J. Phys. Oceanogr.* **29**, 1542–1570 (1999).

40. Dewitte, B., Yeh, S.-W. & Thual, S. Reinterpreting the thermocline feedback in the western-central equatorial Pacific and its relationship with the ENSO modulation. *Clim. Dynam.* **41**, 819–830 (2013).

41. Jin, F.-F. & Neelin, J. D. Modes of interannual tropical ocean–atmosphere interaction—a unified view. Part I: numerical results. *J. Atmos. Sci.* **50**, 3477–3503 (1993).

42. An, S.-I. & Jin, F.-F. Collective role of thermocline and zonal advective feedbacks in ENSO mode. *J. Clim.* **14**, 3241–3432 (2001).

43. An, S.-I. & Jin, F.-F. Nonlinearity and asymmetry of ENSO*. *J. Clim.* **17**, 2399–2412 (2004).

44. Jin, F., Kim, S. T. & Bejarano, L. A coupled-stability index for ENSO. *Geophys. Res. Lett.* **33** (2006).

45. Kug, J., Sooraj, K. -P., Li, T. & Jin, F. Precursors of the El Niño/La Niña onset and their interrelationship. *J. Geophys. Res. Atmos.* **115** (2010).

46. Yun, K.-S. et al. Increasing ENSO–rainfall variability due to changes in future tropical temperature–rainfall relationship. *Commun. Earth Environ.* **2**, 43 (2021).

47. Cornejo-Garrido, A. G. & Stone, P. H. On the heat balance of the walker circulation. *J. Atmos. Sci.* **34**, 1155–1162 (1977).

48. Shukla, J. & Wallace, J. M. Numerical simulation of the atmospheric response to equatorial pacific sea surface temperature anomalies. *J. Atmos. Sci.* **40**, 1613–1630 (1983).

49. Khalsa, S. J. S. The role of sea surface temperature in large-scale air-sea interaction. *Mon. Weather Rev.* **111**, 954–966 (1983).

50. Huang, P. & Xie, S.-P. Mechanisms of change in ENSO-induced tropical Pacific rainfall variability in a warming climate. *Nat. Geosci.* **8**, 922–926 (2015).

51. Lee, S. et al. On the fragile relationship between El Niño and california rainfall. *Geophys. Res. Lett.* **45**, 907–915 (2018).

ACKNOWLEDGEMENTS

AUTHOR CONTRIBUTIONS

N.-Y. Shin compiled the data, conducted analyses, prepared the figures, and wrote the manuscript. J.-S. Kug designed the research and wrote most of the manuscript content. All authors discussed the study results and reviewed the manuscript.

COMPETING INTERESTS

The authors declare no competing interests.

ADDITIONAL INFORMATION

Supplementary information The online version contains supplementary material available at https://doi.org/10.1038/s41612-022-00324-9.

Correspondence and requests for materials should be addressed to Jong-Seong Kug.

Reprints and permission information is available at http://www.nature.com/reprints

Publisher's note Springer Nature remains neutral with regard to jurisdictional claims in published maps and institutional affiliations.